



The High-Effective Catalytic Degradation of Benzo[a]pyrene by Mn-Corrolazine Regulated by Oriented External Electric Field: Insight From DFT Study

Tairen Long¹, Haiyan Wan¹, Jianqiang Zhang², Jie Wu¹, Jin-Xia Liang^{1*} and Chun Zhu^{1*}

¹School of Chemistry and Chemical Engineering, Guizhou University, Guiyang, China, ²Guizhou Fukangren Pharmaceutical Co., Ltd, Guiyang, China

OPEN ACCESS

Edited by:

Liuqingqing Yang,
Shanghai Jiao Tong University, China

Reviewed by:

Ke Yang,
Yale University, United States
Pengfei Tian,
East China University of Science and
Technology, China

*Correspondence:

Jin-Xia Liang
liangjx2009@163.com
Chun Zhu
czhu2014@163.com

Specialty section:

This article was submitted to
Theoretical and Computational
Chemistry,
a section of the journal
Frontiers in Chemistry

Received: 28 February 2022

Accepted: 16 May 2022

Published: 02 June 2022

Citation:

Long T, Wan H, Zhang J, Wu J,
Liang J-X and Zhu C (2022) The High-
Effective Catalytic Degradation of
Benzo[a]pyrene by Mn-Corrolazine
Regulated by Oriented External Electric
Field: Insight From DFT Study.
Front. Chem. 10:884105.
doi: 10.3389/fchem.2022.884105

The degradation of BaP into hydroxybenzo[a]pyrene by Mn-corrolazine and its regulation by an oriented external electronic field (OEEF) were systematically studied using first-principle calculations. Extensive density function calculations showed that the degradation of BaP into hydroxybenzo[a]pyrene by Mn-corrolazine occurs *via* a three-step process in the absence of OEEF, in which a more toxic and stable epoxide intermediate is generated. However, upon application of OEEF along the intrinsic Mn-O reaction axis, the degradation of BaP into hydroxybenzo[a]pyrene is greatly simplified. The negative charge on the terminal O atom of Mn-OO corrolazine increases with an increase in the OEEF intensity. As the intensity of the OEEF increases over 0.004 a.u., the negatively charged terminal O atom has the ability to directly abstract the positively charged H atom of BaP and the degradation of BaP into hydroxybenzo[a]pyrene can be completed *via* a one-step process, avoiding the production of more toxic epoxide intermediates.

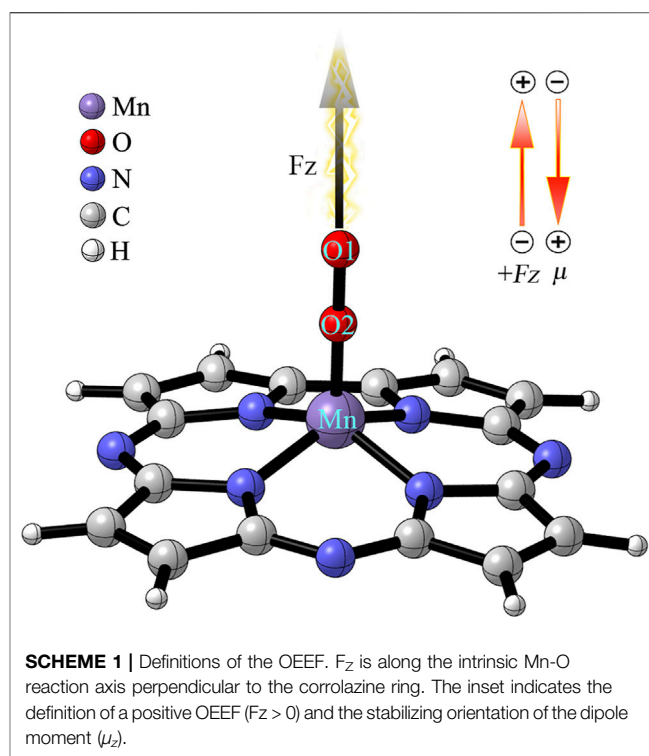
Keywords: benzo[a]pyrene, Mn-corrolazine, catalytic oxidation, density functional theory calculations, oriented external electric field

1 INTRODUCTION

With the development of modern industry, the use of fossil fuels and discharge of soot, flue gas and industrial wastewater have resulted in serious environmental pollution from polycyclic aromatic hydrocarbons (PAHs) (Paulik et al., 2016; Poater et al., 2018; Wu et al., 2018; Yan et al., 2021). As a representative of carcinogenic PAHs, benzo[a]pyrene (BaP) bearing five fused aromatic rings, which is classified as a Group I “human carcinogen” by the World Health Organization (WHO) International Agency for Research on Cancer IARC (2021), has caused irreversible damage to air, water and soil (Lemieux et al., 2015; Strobel et al., 2015; Roberts et al., 2016). Moreover, BaP is persistent organic pollutant, which poses a serious threat to global food security (Średnicka et al., 2021). Seafood with increasing BaP content increases the risk of cancer (Wang et al., 2020) and BaP in roast meat, smoked meat and fried foods will cause serious damage to animals and human organs, such as the liver and kidneys (Takeshita and Kanaly, 2019; Iko Afé et al., 2020; Cunha et al., 2021; Goedtko et al., 2021; Mertens et al., 2021; Ge et al., 2022). Very recent studies (Kostoff et al., 2020) have indicated that people exposed to increased levels of BaP will lead to degradation or dysfunction of the immune system and people will become more susceptible to 2019-nCoV. Therefore, to eliminate the toxicity of BaP, it is essential to study its degradation.

BaP is mainly degraded *via* chemical oxidation, photo-oxidation, microbial degradation and bioaccumulation in the natural environment (Wilson and Jones, 1993; Rubio-Clemente et al., 2018). Among them, the use of bacteria or fungi to biodegrade BaP has received a lot of research attention (Kou et al., 2009; Kuppusamy et al., 2016; Ping et al., 2017; Qin et al., 2017; Delsarte et al., 2018; Gan et al., 2018; Harry-Asobara and Kamei, 2019; Ostrem Loss et al., 2019; Sampaio et al., 2019; Tian et al., 2019), but this approach has a series of drawbacks, such as low catalytic efficiency and difficulty in cultivating suitable bacteria (Wang et al., 2012; Wongwongsee et al., 2013). From the perspective of utilizing solar energy, photocatalysis is one of the most attractive BaP degradation methods reported to date (Kou et al., 2009). BaP can be directly photodegraded upon adsorbing solar energy (Miller and Olejnik, 2001) or degraded using sensitized photochemical reactions (Mill et al., 1981; Fasnacht and Blough, 2002). Recently, the group Luo et al. (2015); Luo et al. (2018) has reported for the first time that natural porphyrins can promote the photoconversion of BaP in water into quinones using singlet oxygen generated *via* a photocatalytic detoxification reaction (Zang et al., 2007). In addition, the possible oxidative degradation mechanisms and pathways of BaP in the atmosphere have been explored by Dang et al. (2015). However, despite the involvement of transition metals in many catalytic processes (Fujihara and Tsuji, 2019; Lin et al., 2021; Parmar et al., 2021; Sánchez-López et al., 2021; Yang et al., 2021; Zhou et al., 2021; Zhou et al., 2022), the use of transition metal complexes as non-sacrificial oxidants for the degradation of BaP has not been reported in the literature.

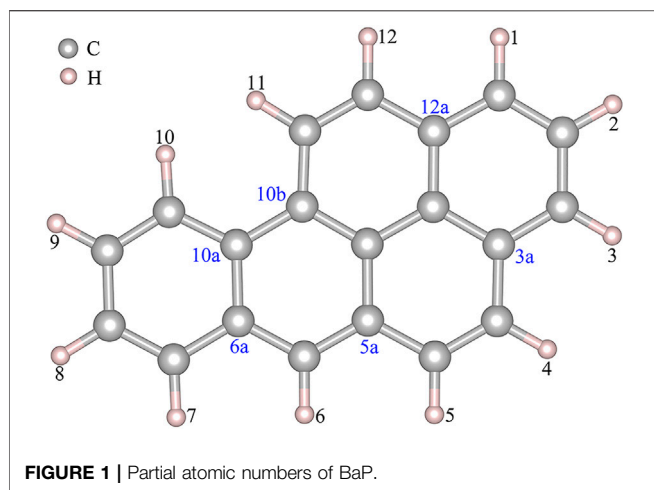
Our group has recently reported that Mn-corrolazine can activate oxygen in the air *via* an electron spin-flip mechanism under visible light irradiation, which forms a singlet [Mn]-O-O species with terminal radical characteristics (Zhu et al., 2018). In fact, corrole has been widely used in many fields (Zhu and Liang, 2015; Zhu et al., 2016; Li and Cao, 2018; Lvova et al., 2018; Liang et al., 2019; Zheng et al., 2020; Dedic et al., 2021; Li et al., 2021). Very recently, oriented external electric fields (OEEFs) have been extensively studied as a ‘smart agent’ by Shaik et al. (2016); (Ramanan et al., 2018; Wang et al., 2018); Shaik et al. (2020). They found that the interaction between OEEFs and dipole moments can change the electron transfer process and enhance the ionicity in the direction of the “reaction axis”, resulting in the regioselectivity of the reaction. Furthermore, our group has also found that OEEFs can effectively regulate the catalytic activity of metal-corrolazines (Wang et al., 2021; Zhu et al., 2021). Therefore, in order to discover a new effective and environmentally-friendly strategy for the degradation of BaP, we have explored the degradation mechanism of BaP to form hydroxybenzo[a]pyrene using Mn-corrolazine involving a [Mn]-O-O species. We further studied the regulation of OEEF on the degradation process. Based on considerable theoretical calculations, we have discovered the reasonable reaction process and OEEF regulation mechanism, which provide a theoretical foundation for further experimental research on the degradation of BaP using Mn-corrolazine regulated by OEEF.



2 COMPUTATIONAL METHODS

The B3LYP density functional method (Lee et al., 1988; Stephens et al., 1994) in combination with an effective core pseudopotential basis set (LANL2DZ) for the Mn atom and 6-31G(d) basis set for all other atoms (B1) was used for all geometry optimizations and frequency calculations performed in the Gaussian 16 package (Frisch et al., 2016). The energies were refined using single-point calculations (Stuyver et al., 2020) utilizing the B3LYP functional with D3BJ dispersion correction (Grimme et al., 2011) coupled with 6-311+G (d,p) (Andersson and Uvdal, 2005) and aug-cc-pVQZ (Mn) (Kendall and Harrison, 1992), i.e., B3LYP-D3(BJ)/6-311+G (d,p), aug-cc-pVQZ (Mn) level of theory (B2). Zero-point energy (ZPE) corrections were taken from the B3LYP/6-31G(d), LANL2DZ (Mn) level of theory. Twelve structures formed by [Mn]-O-O adsorbing different H atoms from BaP were fully optimized to obtain the most stable structure. Based on this structure, the degradation of BaP was studied in which the reactant complexes (RC), transition states (TS), intermediates (IM), and products (P) were fully optimized without any symmetry constraints. Frequency calculations were carried out at the same level of theory in order to assess the nature of a stable point on the potential energy surface and estimate the thermodynamic properties. Moreover, intrinsic reaction coordinate (IRC) analysis was used to further confirm the TS correlating to their corresponding RC and P.

To investigate the effect of OEEF on the reaction, the OEEF F_z along the intrinsic Mn-O reaction axis perpendicular to the corrolazine ring was applied using the keyword “field = M ±



N° , as shown in **Scheme 1**. The positive direction of the electric field vector in **Scheme 1** follows the Gaussian 16 convention. In addition, the electric field strength of F_z was in the range of 0.001–0.01 a.u. (1 a.u. = 51.4 V/Å).

3 RESULTS AND DISCUSSION

3.1 Reactive Site Screening

Figure 1 shows that BaP has 12 H atoms in different chemical environments and in order to find the most reasonable reaction site, we optimized the different RC formed by these 12 different H atoms in BaP and the [Mn]-O-O corrolazines, respectively. **Figure 2** and **Table 1** show that BaP and [Mn]-O-O corrolazine form weak interaction complexes, in which the bond lengths of d_{O1-HX} ($X = 1, 2, 3, \dots, 12$), where the numbers refer to the serial numbers of the H atom, are very similar in the range from 2.537 to 2.845 Å, and the bond length of d_{O1-H11} was the smallest, indicating its interaction was the strongest. Similarly, the energies of these structures are very similar, in which the difference between the highest energy and the lowest energy was only 1.07 kcal/mol, which originates from the weak interaction formed between BaP and [Mn]-O-O corrolazine. In addition, the energy of structure **11** was the lowest, again proving that it was the most stable. Furthermore, **Table 1** shows the bond lengths of Mn-O and O-O were 1.617 and 1.265 Å, respectively, which are similar to the results obtained in

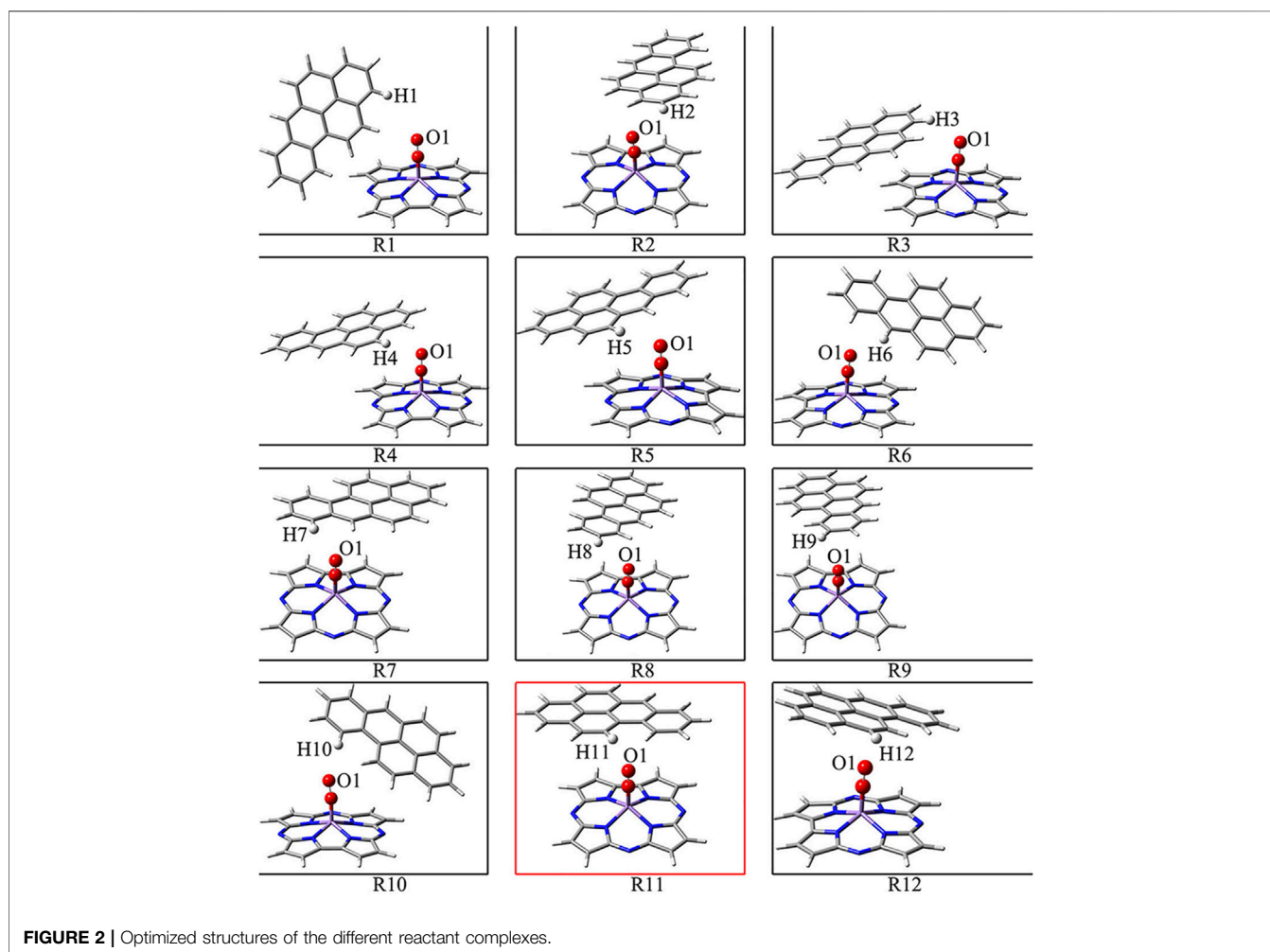


TABLE 1 | |O1-HX (X = 1, 2, 3, ..., 12), Mn-O, O-O bond lengths (Å), relative electronic energies and zero-point energies (ΔE , ΔE_0 , kcal/mol).

Structure	$d_{\text{O1-HX}}(X=1, 2, 3, \dots, 12)$	$d_{\text{Mn-O}}$	$d_{\text{O-O}}$	ΔE	ΔE_0
R1	2.697	1.617	1.264	0.218	0.166
R2	2.776	1.617	1.262	0.792	0.683
R3	2.671	1.617	1.264	0.319	0.263
R4	2.599	1.617	1.263	1.015	0.907
R5	2.608	1.618	1.264	0.953	0.838
R6	2.703	1.619	1.263	0.945	0.809
R7	2.648	1.617	1.264	0.342	0.288
R8	2.845	1.617	1.262	0.725	0.604
R9	2.778	1.617	1.261	0.802	0.684
R10	2.676	1.617	1.263	0.705	0.647
R11	2.537	1.617	1.265	0	0
R12	2.563	1.618	1.264	1.068	0.958

our previous study (Zhu et al., 2018), indicating that the [Mn]-O-O moiety in structure **11** has strong oxidation ability. Therefore, we chose structure **11** as the RC to further explore the degradation of BaP.

3.2 Reaction Mechanism of [Mn]-O-O Catalysed Oxidation of BaP Into 11-OH-BaP

Figure 3 shows [Mn]-O-O corrolazine catalyses the degradation BaP into 11-hydroxybenzo[a]pyrene (11-OH-BaP) *via* three steps: 1) epoxidation, 2) hydrogen transfer

and 3) rearrangement. The first epoxidation step in which 11,12-epoxybenzopyrene (IM1) was generated from BaP. The O-O bond in the [Mn]-O-O moiety was tilted and its terminal O1 attacks the C12 atom in the BaP moiety. The BaP moiety then rotates and its C11 atom attacks the terminal O1 atom to form 11,12-epoxybenzopyrene with a reaction activation energy of 23.3 kcal/mol. During this step, the hybridization of C11 and C12 changes from sp^2 to sp^3 . Following the epoxidation step, IM2 was formed *via* a hydrogen transfer step. In this step, the C11-O1 bond was broken and at the same time, the C11-H11 was broken with H11 being transferred to C12 and C11 returns to sp^2 hybridization. The activation energy of this step was up to 37.98 kcal/mol. The third step was an H atom rearrangement to form 11-OH-BaP (P), in which one H atom on C12 is transferred to O1, followed by a rebound reaction to form P with C12 returning to sp^2 hybridization. In addition, the activation energy in this step was even higher (up to 53.47 kcal/mol). Using whole process analysis, P was the most stable with the lowest energy compared to RC, IM1 and IM2. However, as the activation energies in step 2 and step 3 are very high (37.98 and 53.47 kcal/mol respectively), it is difficult to reach the final product (P) *via* TS2 and TS3. Thus, the reaction will stop at the intermediate product, 11,12-epoxybenzopyrene, which is a carcinogen and even more toxic than BaP. Therefore, it is necessary to seek an efficient way to degrade BaP into the final non-toxic product, 11-OH-BaP.

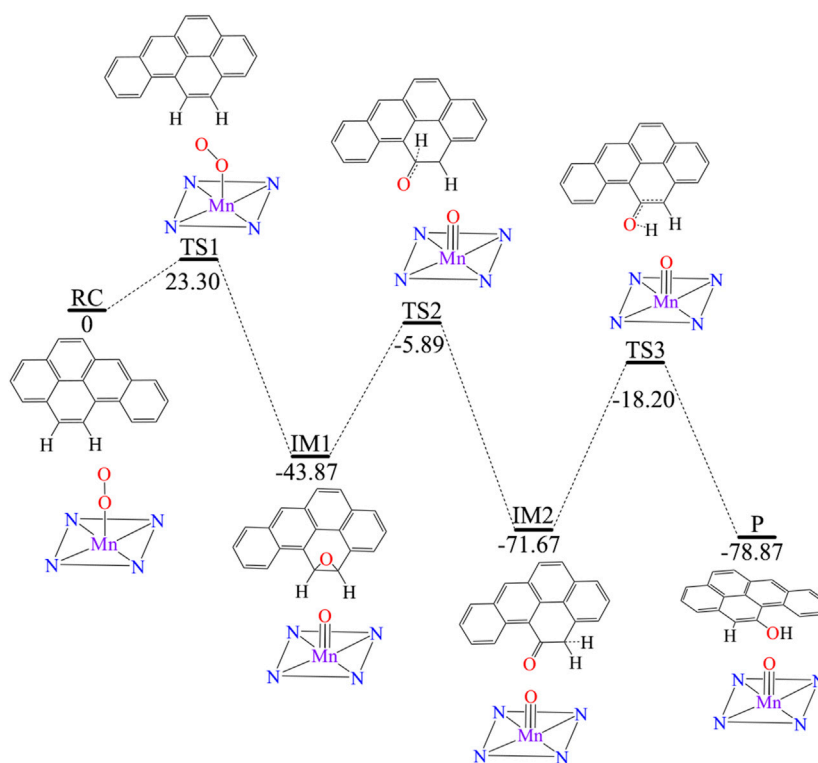
**FIGURE 3** | Predicted reaction pathway for the generation of 11-OH-BaP from BaP *via* [Mn]-O-O corrolazine catalytic oxidation in the absence of an electric field.

TABLE 2 | Variation in the relative electronic energy and dipole moment on the z-axis for the reactants (RC) and transition states (TS) under different electric field strengths in the range of 0–0.01 a.u. Units: ΔE , kcal/mol and μ_z , D.

F_z (10^{-4}) (a.u.)	Complex (ΔE , μ_z)			
	RC (ΔE)	RC (μ_z)	TS (ΔE)	TS (μ_z)
0	0	-2.19	0	5.07
10	0.26	-4.94	1.89	2.27
20	-1.86	-6.46	3.06	2.24
30	-2.51	-7.92	3.47	-1.35
40	-5.53	-10.98	3.32	-6.38
50	-8.84	-12.56	10.58	-9.68
60	-11.53	-13.51	8.28	-11.16
70	-15.14	-15.15	5.27	-13.02
80	-19.17	-16.81	1.81	-14.89
90	-23.52	-18.41	-2.05	-16.67
100	-28.19	-20.05	-6.50	-18.61

3.3 One-step Degradation Mechanism Regulated by OEEF

3.3.1 The Effect of OEEF on the RC and TS

To simplify the reaction process so that BaP can be degraded into 11-OH-BaP in one-step, thereby avoiding the production of highly toxic epoxybenzopyrene, we applied an OEEF F_z along the z-axis, which is the intrinsic Mn-O bond reaction axis perpendicular to the corrolazine ring, in order to regulate the degradation reaction process, as shown in **Scheme 1**.

We first considered the effect of the F_z on the stability of RC in the range of 0–0.01 a.u. **Table 2** and **Figure 4A** show the application of the F_z increases the stability of the RC, in which the relative electronic energy increases upon increasing the electric field intensity. To further explore the reason why the stability of the RC becomes stronger due to the application of the F_z , we analysed the change in the dipole moment in the z-orientation of the RC upon changing the F_z . **Table 2** shows the dipole moment in the z-orientation of the RC increases from -2.19 D without OEEF to -20.05 D in $F_z = 0.01$ a.u. Thus, the enhanced stability of the RC originates from the interaction

between the increased dipole moment in the z-orientation and the F_z .

For the TS, the effect of the OEEF becomes complex, in which different F_z strengths exhibit different behaviour. **Table 2** shows for $F_z < 0.008$ a.u., the OEEF destabilizes the TS upon increasing its relative electronic energy. However, further increasing the intensity of F_z to more than 0.008 a.u., the OEEF stabilizes the TS upon decreasing its relative electronic energy, as shown in the insert of **Figure 4B**. The change in the stabilization can be attributed to the repulsion between the OEEF and increasing dipole moment in the z-orientation of the TS, from 5.07 D without an electric field to 2.24 D in $F_z = 0.002$ a.u. However, further increasing with dipole moment results in the dipole moment in z-orientation flipping its direction at the critical F_z value of 0.003 a.u., and the repulsion between the OEEF and molecular dipole moment in the z-orientation becomes attractive. Thus, the OEEF stabilizes the TS.

3.3.2 The Effect of the OEEF on the Reaction Mechanism

We further investigated the effect of the OEEF on the mechanism of the degradation of BaP into 11-OH-BaP and discovered a very significant phenomenon. The reaction mechanism changes upon increasing the OEEF intensity, i.e., the degradation of BaP into 11-OH-BaP was simplified from a three-step process to a one-step process in which the H11 atom in BaP was directly transferred to the terminal O1 atom in [Mn]-O-O, followed by a rebound reaction of the resulting OH group back to BaP to form 11-OH-BaP, as shown in **Figure 5**. To further explore the reason for the change in the BaP degradation mechanism, we calculated the Mulliken charges of the atoms in the TS involved the H11 atom transfer step. **Table 3** shows the Mulliken charge at O1 was -0.203 |e| without the OEEF. As the F_z strength increases from 0 to 0.004 a.u., the Mulliken charge of the O1 atom increases from -0.21 |e| to -0.30 |e|, increasing its attraction to the positively charged H11 atom. However, the BaP moiety in

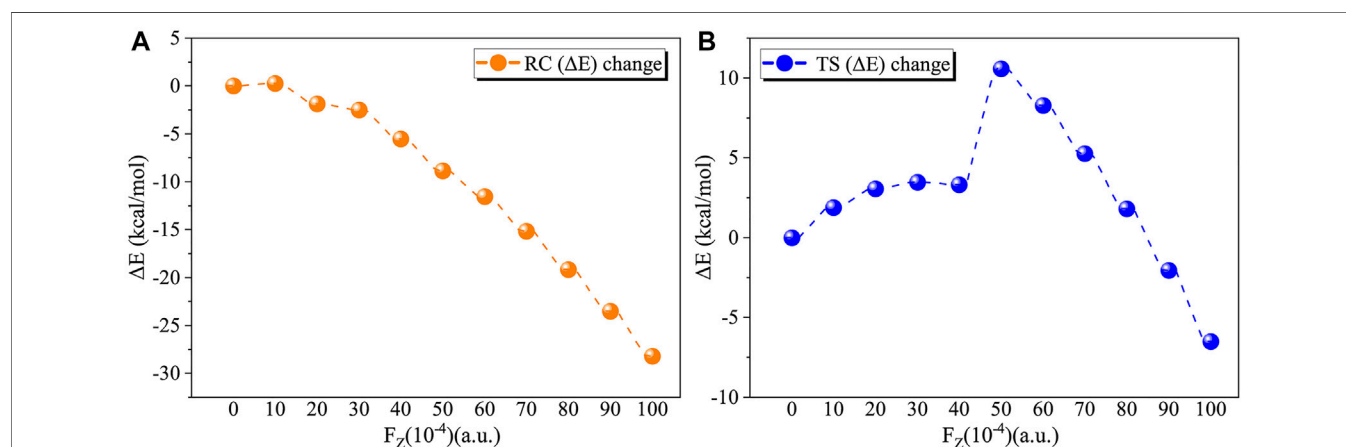
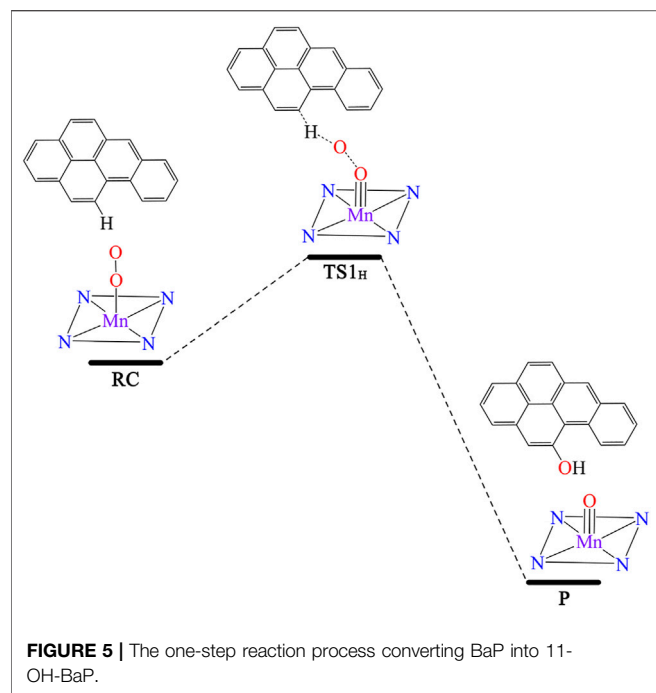


FIGURE 4 | (A) Variation in the relative electron energy of the reactants (RC) with the electric field strength. (B) Variation in the relative electron energy of the transition states (TS) with the electric field strength.



the reactant complex rotates continuously in this process, from almost parallel to the Mn-O bond to almost perpendicular to the Mn-O bond, so that the effect of the OEEF parallel to the Mn-O bond on BaP initially increases and then decreases. Therefore, the Mulliken charge on the H11 atom first increases from 0.175 |e| at $F_z = 0$ to 0.179 |e| at $F_z = 0.002$ a.u., and then decreases to 0.144 |e| at $F_z = 0.004$ a.u., which is the minimum value. In addition, the attraction of the negatively charged terminal O1 atom to the positively charged H11 atom was also weakened. Therefore, the reaction mechanism remains a three-step process, in which the terminal O1 atom is attracted to the C12 atom to form an epoxybenzopyrene intermediate. However, further increasing the OEEF intensity increases the negative charge on the terminal O1 atom to be more than 0.3 |e|. At the same time, the BaP moiety further rotates and deviates from direction parallel to the Mn-O bond, so the effect of the OEEF on BaP moiety was significantly strengthened and the positive charge on the H11 atom increases sharply. Moreover, as the positive charge of H11 exceeds that of C12, the interaction between H11 and the terminal O1 atom is stronger than that between C12 and O1, resulting in the TS to change from O1 attacking C12 to O1 attacking H11. Due to the change in the TS, the H11 atom can be directly transferred to the O1 atom to form 11-OH-BaP via a subsequent rebound reaction. Thus, the degradation of BaP into 11-OH-BaP was greatly simplified from a one-step to three-step process. Moreover, the simplified degradation reaction of BaP avoids the production of toxic epoxybenzopyrene.

Analysis of the reaction activation energy of the degradation reaction of BaP into 11-OH-BaP upon the

TABLE 3 | Mulliken charges (|e|) of some atoms in the reactive centre of the transition state and activation energies ΔE_0 (electronic energies + ZPE: kcal/mol) under an electric field.

F_z (10^{-4}) (a.u.)	O1	H11	C12	Activation energy
0	-0.203	0.175	-0.170	23.30
10	-0.216	0.171	-0.160	17.32
20	-0.210	0.179	-0.168	21.37
30	-0.230	0.166	-0.151	21.42
40	-0.300	0.144	-0.164	17.03
50	-0.357	0.276	-0.179	28.80
60	-0.362	0.280	-0.181	29.07
70	-0.368	0.285	-0.183	29.58
80	-0.374	0.291	-0.184	30.07
90	-0.379	0.294	-0.185	30.50
100	-0.386	0.299	-0.185	30.92

application of the OEEF shows its effect on the RC and TS was similar in the first step with the reaction activation energy varying slightly from $F_z = 0$ to $F_z = 0.004$ a.u. When the F_z was increased from 0.004 to 0.005 a.u., the reaction activation energy increases sharply from 17.03 to 28.80 kcal/mol due to the fundamental change in the TS. However, further increasing the OEEF from $F_z = 0.005$ to $F_z = 0.01$ a.u., the reaction activation increases slightly because the structure of the TS remains unchanged. Analysis of the whole reaction process shows that the reaction activation energy of the one-step process in $F_z > 0.005$ a.u. was higher than that in the first step of the three-step process and the activation energy of the one-step process was significantly less than those of the second and third step in the three-step process. Therefore, the regulation of the OEEF significantly simplifies the degradation reaction of BaP to an effective and environmentally-friendly process, which is of great significance to the food industry.

4 CONCLUSION

BaP is widely found in the natural environment and food, etc., and its degradation is of great significance for biosafety because of its carcinogenicity as a Group I “human carcinogen”. We have used Mn-OO corrolazine to degrade BaP into 11-OH-BaP in order to detoxify it. The degradation process occurs via a three-step process under field-free condition, i.e., epoxidation, hydrogen transfer and rearrangement, in which a more toxic epoxide intermediate is produced. Due to the high stability of the epoxide intermediate with an activation energy of up to 53.47 kcal/mol for further reaction, BaP is difficult to degrade into 11-OH-BaP using [Mn]-O-O corrolazine. However, the application of an OEEF along the intrinsic Mn-O reaction axis, which is more easily aligned in practical applications, greatly simplified the degradation of BaP into 11-OH-BaP. As the OEEF can effectively regulate the charge on the terminal O atom in [Mn]-O-O corrolazine, the H atom in BaP can be directly attracted by the terminal O atom to generate 11-OH-BaP via a subsequent rebound reaction. Thus, the complex

three-step degradation process of BaP into 11-OH-BaP has been simplified into a one-step process, avoiding the generation of the more toxic and stable epoxide intermediate. This effective and environmentally-friendly degradation process will have a far-reaching impact on areas such as the environment and food industry.

DATA AVAILABILITY STATEMENT

The original contributions presented in the study are included in the article/supplementary material, further inquiries can be directed to the corresponding authors.

REFERENCES

- Andersson, M. P., and Uvdal, P. (2005). New Scale Factors for Harmonic Vibrational Frequencies Using the B3LYP Density Functional Method with the Triple- ζ Basis Set 6-311+G(d,p). *J. Phys. Chem. A* 109, 2937–2941. doi:10.1021/jp045733a
- Cunha, S. C., Siminel, D., Guárdia, M. D., de Alda, M. L., López-García, E., Muñoz, I., et al. (2021). Effect of Processing Smoked Salmon on Contaminant Contents. *Food Chem. Toxicol.* 153, 112276. doi:10.1016/j.fct.2021.112276
- Dang, J., Shi, X., Hu, J., Chen, J., Zhang, Q., and Wang, W. (2015). Mechanistic and Kinetic Studies on OH-initiated Atmospheric Oxidation Degradation of Benzo [a]pyrene in the Presence of O₂ and NO_x. *Chemosphere* 119, 387–393. doi:10.1016/j.chemosphere.2014.07.001
- Dedic, D., Dorniak, A., Rinner, U., and Schöfberger, W. (2021). Recent Progress in (Photo-)Electrochemical Conversion of CO₂ with Metal Porphyrinoid-Systems. *Front. Chem.* 9, 685619. doi:10.3389/fchem.2021.685619
- Delsarte, I., Rafin, C., Mrad, F., and Veignie, E. (2018). Lipid Metabolism and Benzo[a]pyrene Degradation by *Fusarium Solani*: an Unexplored Potential. *Environ. Sci. Pollut. Res.* 25, 12177–12182. doi:10.1007/s11356-017-1164-y
- Fasnacht, M. P., and Blough, N. V. (2002). Aqueous Photodegradation of Polycyclic Aromatic Hydrocarbons. *Environ. Sci. Technol.* 36, 4364–4369. doi:10.1021/es025603k
- Frisch, M. J., Trucks, G. W., Schlegel, H. B., Scuseria, G. E., Robb, M. A., Cheeseman, J. R., et al. (2016). *Gaussian 16, Revision B.01*. Wallingford, CT: Gaussian, Inc.
- Fujihara, T., and Tsuji, Y. (2019). Carboxylation Reactions Using Carbon Dioxide as the C1 Source via Catalytically Generated Allyl Metal Intermediates. *Front. Chem.* 7, 430. doi:10.3389/fchem.2019.00430
- Gan, X., Teng, Y., Zhao, L., Ren, W., Chen, W., Hao, J., et al. (2018). Influencing Mechanisms of Hematite on Benzo(a)pyrene Degradation by the PAH-Degrading Bacterium *Paracoccus* Sp. Strain HPD-2: Insight from Benzo(a)pyrene Bioaccessibility and Bacteria Activity. *J. Hazard. Mater.* 359, 348–355. doi:10.1016/j.jhazmat.2018.07.070
- Ge, J., Hao, R., Rong, X., Dou, Q. P., Tan, X., Li, G., et al. (2022). Secoisolariciresinol Diglucoside Mitigates Benzo[a]pyrene-Induced Liver and Kidney Toxicity in Mice via miR-101a/MKP-1-Mediated P38 and ERK Pathway. *Food Chem. Toxicol.* 159, 112733. doi:10.1016/j.fct.2021.112733
- Goedtke, L., John, A., Lampen, A., Seidel, A., Braeuning, A., and Hessel-Pras, S. (2021). Mixture Effects of Food-Relevant Polycyclic Aromatic Hydrocarbons on the Activation of Nuclear Receptors and Gene Expression, Benzo[a]pyrene Metabolite Profile and DNA Damage in HepaRG Cells. *Food Chem. Toxicol.* 147, 111884. doi:10.1016/j.fct.2020.111884
- Grimme, S., Ehrlich, S., and Goerigk, L. (2011). Effect of the Damping Function in Dispersion Corrected Density Functional Theory. *J. Comput. Chem.* 32, 1456–1465. doi:10.1002/jcc.21759
- Harry-Asobara, J. L., and Kamei, I. (2019). Growth Management of White-Rot Fungus *Phlebia Brevispora* Improved Degradation of High-Molecular-Weight

AUTHOR CONTRIBUTIONS

TL: investigation, Writing-original draft. HW: investigation. JZ: investigation. JW: investigation, discussed the data. J-XL: investigation, supervision, writing-review and editing, project. CZ: supervision, writing-review and editing, project administration, funding acquisition.

FUNDING

This work was supported by the National Science Foundation of China (No. 21963005 and 21763006), Natural Science Foundation of Guizhou University [No. (2021)40 and (2020)32].

Polycyclic Aromatic Hydrocarbons. *3 Biotech.* 9, 403. doi:10.1007/s13205-019-1932-0

IARC (2021). Monographs on the Evaluation of Carcinogenic Risks to Humans. Available at: <http://monographs.iarc.fr/ENG/Classification/> (accessed December 8, 2021).

Iko Afé, O. H., Douny, C., Kpoclou, Y. E., Igout, A., Mahillon, J., Anihouvi, V., et al. (2020). Insight about Methods Used for Polycyclic Aromatic Hydrocarbons Reduction in Smoked or Grilled Fishery and Meat Products for Future Re-engineering: A Systematic Review. *Food Chem. Toxicol.* 141, 111372. doi:10.1016/j.fct.2020.111372

Kendall, R. A., Jr., Dunning, T. H., and Harrison, R. J. (1992). Electron Affinities of the First-row Atoms Revisited. Systematic Basis Sets and Wave Functions. *J. Chem. Phys.* 96, 6796–6806. doi:10.1063/1.462569

Kostoff, R. N., Briggs, M. B., Porter, A. L., Hernández, A. F., Abdollahi, M., Aschner, M., et al. (2020). The Under-reported Role of Toxic Substance Exposures in the COVID-19 Pandemic. *Food Chem. Toxicol.* 145, 111687. doi:10.1016/j.fct.2020.111687

Kou, J., Li, Z., Yuan, Y., Zhang, H., Wang, Y., and Zou, Z. (2009). Visible-Light-Induced Photocatalytic Oxidation of Polycyclic Aromatic Hydrocarbons over Tantalum Oxynitride Photocatalysts. *Environ. Sci. Technol.* 43, 2919–2924. doi:10.1021/es802940a

Kuppusamy, S., Thavamani, P., Megharaj, M., Lee, Y. B., and Naidu, R. (2016). Kinetics of PAH Degradation by a New Acid-Metal-Tolerant *Trabulsiella* Isolated from the MGP Site Soil and Identification of its Potential to Fix Nitrogen and Solubilize Phosphorous. *J. Hazard. Mater.* 307, 99–107. doi:10.1016/j.jhazmat.2015.12.068

Lee, C., Yang, W., and Parr, R. G. (1988). Development of the Colle-Salvetti Correlation-Energy Formula into a Functional of the Electron Density. *Phys. Rev. B* 37, 785–789. doi:10.1103/PhysRevB.37.785

Lemieux, C. L., Long, A. S., Lambert, I. B., Lundstedt, S., Tysklind, M., and White, P. A. (2015). Cancer Risk Assessment of Polycyclic Aromatic Hydrocarbon Contaminated Soils Determined Using Bioassay-Derived Levels of Benzo[a]pyrene Equivalents. *Environ. Sci. Technol.* 49, 1797–1805. doi:10.1021/es504466b

Li, P., and Cao, Z. (2018). Catalytic Preparation of Cyclic Carbonates from CO₂ and Epoxides by Metal-Porphyrin and -Corrole Complexes: Insight into Effects of Cocatalyst and Meso-Substitution. *Organometallics* 37, 406–414. doi:10.1021/acs.organomet.7b00830

Li, X., Zhang, X.-P., Guo, M., Lv, B., Guo, K., Jin, X., et al. (2021). Identifying Intermediates in Electrocatalytic Water Oxidation with a Manganese Corrole Complex. *J. Am. Chem. Soc.* 143, 14613–14621. doi:10.1021/jacs.1c05204

Liang, J.-X., Wu, Y., Deng, H., Long, C., and Zhu, C. (2019). Theoretical Investigation on the Electronic Structure of One Dimensional Infinite Monatomic Gold Wire: Insights into Conducting Properties. *RSC Adv.* 9, 1373–1377. doi:10.1039/C8RA08286C

Lin, K., Shi, A., Shi, C., Lin, J., and Lin, H. (2021). Catalytic Asymmetric Amino Acid and its Derivatives by Chiral Aldehyde Catalysis. *Front. Chem.* 9, 687817. doi:10.3389/fchem.2021.687817

- Luo, L., Lai, X., Chen, B., Lin, L., Fang, L., Tam, N. F. Y., et al. (2015). Chlorophyll Catalyse the Photo-Transformation of Carcinogenic Benzo[a]pyrene in Water. *Sci. Rep.* 5, 12776. doi:10.1038/srep12776
- Luo, L., Xiao, Z., Chen, B., Cai, F., Fang, L., Lin, L., et al. (2018). Natural Porphyrins Accelerating the Phototransformation of Benzo[a]pyrene in Water. *Environ. Sci. Technol.* 52, 3634–3641. doi:10.1021/acs.est.7b05854
- Lvova, L., Caroleo, F., Garau, A., Lippolis, V., Giorgi, L., Fusi, V., et al. (2018). A Fluorescent Sensor Array Based on Heteroatomic Macrocyclic Fluorophores for the Detection of Polluting Species in Natural Water Samples. *Front. Chem.* 6, 258. doi:10.3389/fchem.2018.00258
- Mertens, B., Van Heyst, A., Demaegdt, H., Boonen, I., Van Den Houwe, K., Gosciny, S., et al. (2021). Assessment of Hazards and Risks Associated with Dietary Exposure to Mineral Oil for the Belgian Population. *Food Chem. Toxicol.* 149, 112034. doi:10.1016/j.fct.2021.112034
- Mill, T., Mabey, W. R., Lan, B. Y., and Baraze, A. (1981). Photolysis of Polycyclic Aromatic Hydrocarbons in Water. *Chemosphere* 10, 1281–1290. doi:10.1016/0045-6535(81)90045-X
- Miller, J. S., and Olejnik, D. (2001). Photolysis of Polycyclic Aromatic Hydrocarbons in Water. *Water Res.* 35, 233–243. doi:10.1016/S0043-1354(00)00230-X
- Ostrem Loss, E. M., Lee, M.-K., Wu, M.-Y., Martien, J., Chen, W., Amador-Noguez, D., et al. (2019). Cytochrome P450 Monooxygenase-Mediated Metabolic Utilization of Benzo[a]Pyrene by *Aspergillus* Species. *Mbio* 10, e00558–00519. doi:10.1128/mBio.00558-19
- Parmar, S. V., Avasare, V., and Pal, S. (2021). Unraveling the Effect of Aromatic Groups in Mn(II)NNN Pincer Complexes on Carbon Dioxide Activation Using Density Functional Study. *Front. Chem.* 9, 778718. doi:10.3389/fchem.2021.778718
- Paulik, L. B., Donald, C. E., Smith, B. W., Tidwell, L. G., Hobbie, K. A., Kincl, L., et al. (2016). Emissions of Polycyclic Aromatic Hydrocarbons from Natural Gas Extraction into Air. *Environ. Sci. Technol.* 50, 7921–7929. doi:10.1021/acs.est.6b02762
- Ping, L., Guo, Q., Chen, X., Yuan, X., Zhang, C., and Zhao, H. (2017). Biodegradation of Pyrene and Benzo[a]pyrene in the Liquid Matrix and Soil by a Newly Identified *Raoultella Planticola* Strain. *3 Biotech.* 7, 56. doi:10.1007/s13205-017-0704-y
- Poater, J., Duran, M., and Solà, M. (2018). Aromaticity Determines the Relative Stability of Kinked vs. Straight Topologies in Polycyclic Aromatic Hydrocarbons. *Front. Chem.* 6, 561. doi:10.3389/fchem.2018.00561
- Qin, W., Zhu, Y., Fan, F., Wang, Y., Liu, X., Ding, A., et al. (2017). Biodegradation of Benzo(a)pyrene by Microbacterium Sp. Strain under Denitrification: Degradation Pathway and Effects of Limiting Electron Acceptors or Carbon Source. *Biochem. Eng. J.* 121, 131–138. doi:10.1016/j.bej.2017.02.001
- Ramanan, R., Danovich, D., Mandal, D., and Shaik, S. (2018). Catalysis of Methyl Transfer Reactions by Oriented External Electric Fields: Are Gold-Thiolate Linkers Innocent? *J. Am. Chem. Soc.* 140, 4354–4362. doi:10.1021/jacs.8b00192
- Roberts, S. M., Munson, J. W., Ruby, M. V., and Lowney, Y. (2016). Effects of Source and Concentration on Relative Oral Bioavailability of Benzo(a) pyrene from Soil. *Environ. Sci. Technol.* 50, 11274–11281. doi:10.1021/acs.est.6b01534
- Rubio-Clemente, A., Chica, E., and Peñuela, G. A. (2018). Photovoltaic Array for Powering Advanced Oxidation Processes: Sizing, Application and Investment Costs for the Degradation of a Mixture of Anthracene and Benzo[a]pyrene in Natural Water by the UV/H₂O₂ System. *J. Environ. Chem. Eng.* 6, 2751–2761. doi:10.1016/j.jece.2018.03.046
- Sampaio, C. J. S., de Souza, J. R. B., Damião, A. O., Bahiense, T. C., and Roque, M. R. A. (2019). Biodegradation of Polycyclic Aromatic Hydrocarbons (PAHs) in a Diesel Oil-Contaminated Mangrove by Plant Growth-Promoting Rhizobacteria. *3 Biotech.* 9, 155. doi:10.1007/s13205-019-1686-8
- Sánchez-López, P., Kotolevich, Y., Yocupicio-Gaxiola, R. I., Antúnez-García, J., Chowdari, R. K., Petranovskii, V., et al. (2021). Recent Advances in Catalysis Based on Transition Metals Supported on Zeolites. *Front. Chem.* 9, 716745. doi:10.3389/fchem.2021.716745
- Shaik, S., Danovich, D., Joy, J., Wang, Z., and Stuyver, T. (2020). Electric-Field Mediated Chemistry: Uncovering and Exploiting the Potential of (Oriented) Electric Fields to Exert Chemical Catalysis and Reaction Control. *J. Am. Chem. Soc.* 142, 12551–12562. doi:10.1021/jacs.0c05128
- Shaik, S., Mandal, D., and Ramanan, R. (2016). Oriented Electric Fields as Future Smart Reagents in Chemistry. *Nat. Chem.* 8, 1091–1098. doi:10.1038/nchem.2651
- Średnicka, P., Juszczuk-Kubiak, E., Wójcicki, M., Akimowicz, M., and Roszko, M. L. (2021). Probiotics as a Biological Detoxification Tool of Food Chemical Contamination: A Review. *Food Chem. Toxicol.* 153, 112306. doi:10.1016/j.fct.2021.112306
- Stephens, P. J., Devlin, F. J., Chabalowski, C. F., and Frisch, M. J. (1994). Ab Initio Calculation of Vibrational Absorption and Circular Dichroism Spectra Using Density Functional Force Fields. *J. Phys. Chem.* 98, 11623–11627. doi:10.1021/j100096a001
- Strobel, A., Burkhardt-Holm, P., Schmid, P., and Segner, H. (2015). Benzo(a) pyrene Metabolism and EROD and GST Biotransformation Activity in the Liver of Red- and White-Blooded Antarctic Fish. *Environ. Sci. Technol.* 49, 8022–8032. doi:10.1021/acs.est.5b00176
- Stuyver, T., Ramanan, R., Mallick, D., and Shaik, S. (2020). Oriented (Local) Electric Fields Drive the Millionfold Enhancement of the H-Abstraction Catalysis Observed for Synthetic Metalloenzyme Analogues. *Angew. Chem. Int. Ed.* 59, 7915–7920. doi:10.1002/anie.201916592
- Takeshita, T., and Kanaly, R. A. (2019). *In Vitro* DNA/RNA Adductomics to Confirm DNA Damage Caused by Benzo[a]pyrene in the Hep G2 Cell Line. *Front. Chem.* 7, 491. doi:10.3389/fchem.2019.00491
- Tian, F., Guo, G., Ding, K., Wang, L., Liu, T., and Yang, F. (2019). Effect of Bioaugmentation by Bacterial Consortium and Methyl- β -Cyclodextrin on Soil Functional Diversity and Removal of Polycyclic Aromatic Hydrocarbons. *Polycycl. Aromat. Compd.* 39, 353–362. doi:10.1080/10406638.2017.1326952
- Wang, H., Huang, W., Gong, Y., Chen, C., Zhang, T., and Diao, X. (2020). Occurrence and Potential Health Risks Assessment of Polycyclic Aromatic Hydrocarbons (PAHs) in Different Tissues of Bivalves from Hainan Island, China. *Food Chem. Toxicol.* 136, 111108. doi:10.1016/j.fct.2019.111108
- Wang, S., Li, X., Liu, W., Li, P., Kong, L., Ren, W., et al. (2012). Degradation of Pyrene by Immobilized Microorganisms in Saline-Alkaline Soil. *J. Environ. Sci.* 24, 1662–1669. doi:10.1016/s1001-0742(11)60963-7
- Wang, X., Wang, H., Zheng, L., Zhu, C., and Liang, J. X. (2021). Oriented External Electric Fields Regulating the Oxidation Reaction of CH₄ Catalyzed by Mn-corrolazine. *Int. J. Quantum Chem.* 121, e26443. doi:10.1002/qua.26443
- Wang, Z., Danovich, D., Ramanan, R., and Shaik, S. (2018). Oriented-External Electric Fields Create Absolute Enantioselectivity in Diels-Alder Reactions: Importance of the Molecular Dipole Moment. *J. Am. Chem. Soc.* 140, 13350–13359. doi:10.1021/jacs.8b08233
- Wilson, S. C., and Jones, K. C. (1993). Bioremediation of Soil Contaminated with Polynuclear Aromatic Hydrocarbons (PAHs): a Review. *Environ. Pollut.* 81, 229–249. doi:10.1016/0269-7491(93)90206-4
- Wongwongsee, W., Chareanpat, P., and Pinyakong, O. (2013). Abilities and Genes for PAH Biodegradation of Bacteria Isolated from Mangrove Sediments from the Central of Thailand. *Mar. Pollut. Bull.* 74, 95–104. doi:10.1016/j.marpolbul.2013.07.025
- Wu, D., Li, Q., Ding, X., Sun, J., Li, D., Fu, H., et al. (2018). Primary Particulate Matter Emitted from Heavy Fuel and Diesel Oil Combustion in a Typical Container Ship: Characteristics and Toxicity. *Environ. Sci. Technol.* 52, 12943–12951. doi:10.1021/acs.est.8b04471
- Yan, X., Wang, Y., Meng, T., and Yan, H. (2021). Computational Insights into the Influence of Substitution Groups on the Inclusion Complexation of β -Cyclodextrin. *Front. Chem.* 9, 668400. doi:10.3389/fchem.2021.668400
- Yang, L., Pastor-Pérez, L., Villora-Pico, J. J., Sepúlveda-Escribano, A., Tian, F., Zhu, M., et al. (2021). Highly Active and Selective Multicomponent Fe-Cu/CeO₂-Al₂O₃ Catalysts for CO₂ Upgrading via RWGS: Impact of Fe/Cu Ratio. *ACS Sustain. Chem. Eng.* 9, 12155–12166. doi:10.1021/acssuschemeng.1c03551
- Zang, S.-y., Li, P.-j., Yu, X.-c., Shi, K., Zhang, H., and Chen, J. (2007). Degradation of Metabolites of Benzo[a]pyrene by Coupling Penicillium chrysogenum with KMnO₄. *J. Environ. Sci.* 19, 238–243. doi:10.1016/S1001-0742(07)60039-4
- Zheng, L., Meng, Y., Wang, X., Zhu, C., and Liang, J.-X. (2020). Screening Metal-Dicorrole-Based Dyes with Excellent Photoelectronic Properties for Dye-Sensitized Solar Cells by Density Functional Calculations. *J. Porphyr. Phthalocyanines* 24, 1003–1012. doi:10.1142/s1088424620500145
- Zhou, C., Zhang, H., Yang, L., Wu, D., He, S., Yang, H., et al. (2022). Methane-selective Oxidation to Methanol and Ammonia Selective Catalytic Reduction of

- NO_x over Monolithic Cu/SSZ-13 Catalysts: Are Hydrothermal Stability and Active Sites Same? *Fuel* 309, 122178. doi:10.1016/j.fuel.2021.122178
- Zhou, J., Zhao, Z., and Shibata, N. (2021). Silylboronate-Mediated Defluorosilylation of Aryl Fluorides with or without Ni-Catalyst. *Front. Chem.* 9, 771473. doi:10.3389/fchem.2021.771473
- Zhu, C., Liang, J.-X., and Cao, Z. (2018). Mn-O-O Electron Spin Flip Mechanism Triggered by the Visible-Light Irradiation for the Generation of an Active Mn(V)-Oxo Complex from O₂: Insight from Density Functional Calculations. *J. Phys. Chem. C* 122, 20781–20786. doi:10.1021/acs.jpcc.8b05531
- Zhu, C., Liang, J.-X., Meng, Y., Lin, J., and Cao, Z. (2021). Mn-corrrolazine-based 2D-Nanocatalytic Material with Single Mn Atoms for Catalytic Oxidation of Alkane to Alcohol. *Chin. J. Catal.* 42, 1030–1039. doi:10.1016/S1872-2067(20)63707-X
- Zhu, C., and Liang, J.-X. (2015). Theoretical Insight into the Interaction between Gallium Di-corrrole Dyes and Iodine in Dye-Sensitized Solar Cells (DSCs). *J. Power Sources* 283, 343–350. doi:10.1016/j.jpowsour.2015.02.136
- Zhu, C., Liang, J.-X., and Wei, G. (2016). Theoretical Investigation of an Ultrastable One Dimensional Infinite Monatomic Mixed Valent Gold Wire with Excellent Electronic Properties. *Phys. Chem. Chem. Phys.* 18, 12338–12343. doi:10.1039/c6cp00787b

Conflict of Interest: Author JZ is employed by Guizhou Fukangren Pharmaceutical Co., LTD.

The remaining authors declare that the research was conducted in the absence of any commercial or financial relationships that could be construed as a potential conflict of interest.

Publisher's Note: All claims expressed in this article are solely those of the authors and do not necessarily represent those of their affiliated organizations, or those of the publisher, the editors and the reviewers. Any product that may be evaluated in this article, or claim that may be made by its manufacturer, is not guaranteed or endorsed by the publisher.

Copyright © 2022 Long, Wan, Zhang, Wu, Liang and Zhu. This is an open-access article distributed under the terms of the Creative Commons Attribution License (CC BY). The use, distribution or reproduction in other forums is permitted, provided the original author(s) and the copyright owner(s) are credited and that the original publication in this journal is cited, in accordance with accepted academic practice. No use, distribution or reproduction is permitted which does not comply with these terms.